Assessing and Visualizing Uncertainty of 3D Geological Surfaces Using Level Sets with Stochastic Motion

Liang Yang[a], David Hyde[b], Ognjen Grujic[a], Celine Scheidt[c], Jef Caers[a]

[a]*Department of Geological Sciences, Stanford University; 367 Panama Street, Stanford, CA 94305, USA*
[b]*Department of Computer Science, Stanford University; 353 Serra Mall, Stanford, CA 94305, USA*
[c]*Department of Energy Resources Engineering, Stanford University; 367 Panama Street, Stanford, CA 94305, USA*

Abstract

For many geoscience applications, prediction requires building complex 3D surface models. Because of such complexity, often only a single model is built, possibly with a small set of variants to represent the uncertainty. Recent advancement in implicit modeling has made the construction of 3D geological models simpler; however, automatic assessment and visualization of uncertainty constrained by input geological rules and data constraints is still an active research topic. In this paper, we propose a new method that directly assesses and visualizes the uncertainty of geological surfaces by the means of stochastic motion. We represent the geological surfaces as the addition of stochastic implicit conceptual models and residual functions subject to the constraints of data and geological age relationships. Two sampling approaches to create the stochastic motion are proposed: Monte Carlo and Markov chain Monte Carlo (McMC). The uncertainty is assessed by independent realizations drawn by Monte Carlo sampling. The uncertainty is visualized by a "smooth" movie of gradually evolving geological surfaces that have the same stationary distribution as Monte Carlo, sampled by Markov chain Monte Carlo (McMC). This idea is integrated into the level set equation. Level sets are an ideal way to represent mathematically complex surfaces without explicit grid representations, thereby having the advantage of avoiding tedious topological computations such as defining the connectivity of a surface. We illustrate this new idea with simple synthetic 3D examples, taking the constraints of data and geological age relationships into consideration. Finally, we illustrate the idea using a synthetic data set from a copper deposit, where dense drillholes constrain an ore body with seven different lithologies. Our method provides a direct assessment and visualization of the uncertainty of 3D geological surfaces.

Keywords: 3D Geological models, gradual deformation, Markov chain Monte Carlo, conditional simulation

---

1. Introduction and Related Work

Building 3D geological models is crucial in subsurface prediction and risk assessment. Model building is widely applied in reservoir forecasting (Thore et al., 2002), mining planning (Cowan et al., 2003), groundwater assessment (Hassen et al., 2016) and civil engineering (Hou et al., 2016).

Many geological modeling exercises require building 3D surfaces of geological structures (e.g., ore bodies, reservoirs, faults). Due to the sparsity and imprecision of geological data, as well as a lack of geological understanding, uncertainty is an integral property of 3D surface models (Caumon, 2010; Mallet, 2014; Wellmann et al., 2010). Assessing and visualizing the uncertainty of these 3D surfaces have been acknowledged to be important and challenging tasks (Caers, 2011; Caumon, 2010; Lindsay et al., 2013; Scheidt et al., 2018).

Traditionally, uncertainty models are constructed with explicit methods, but the topology is fixed for all realizations (Lecour et al., 2001; Thore et al., 2002). This limitation is due to the fact that explicit methods require tedious manual effort to define the topology, such as the connectivity of a single surface and the spatial relationship among multiple surfaces. Thus, with explicit methods, it is almost impossible to edit the topology for every single realization. Implicit methods, which use level sets to represent surfaces, were applied to model geological structures as early as Lajaunie et al. (1997) and have since gained considerable attention in geological modeling because little manual intervention is required in the modeling process (Calcagno et al., 2008; Caumon et al., 2013; Cowan et al., 2003; Gonçalves et al., 2017; Frank et al., 2007; Vollgger et al., 2015). Although implicit methods usually focus on interpolating a single deterministic model, they have the advantage of handling topological perturbations naturally, rendering future work about the joint quantification of geometric and topological uncertainty a feasible and automatic task (Aydin and Caers, 2017; Cherpeau and Caumon, 2015).

In general, two avenues have been explored for uncertainty assessment on 3D surfaces. One is base-case reasoning, which involves either estimating uncertainty based on the kriging variance (Chilès et al., 2004; Tacher et al., 2006), or perturbing a reference (base) model to generate multiple realizations (Caumon et al., 2007; Lecour et al., 2001; Mallet, 2014; Røe et al., 2014; Thore et al., 2002). Some base-case reasoning approaches specify an uncertainty boundary and perturb the base model within that boundary (Caumon et al., 2007; Lecour et al., 2001; Røe et al., 2014; Thore et al., 2002). Others consider the "coherency" among realizations while perturbing the base model (Mallet, 2014). The base-case reasoning approach has potential drawbacks; for instance, the base model may be biased, and the uncertainty of key prediction variables may be underestimated. However, for some applications where dense data sets (e.g., numerous drillholes) are available, such as mineral resources forecasting, the drawback may be alleviated, and it has compuational advantages compared to the other avenue, fully stochastic. A fully stochastic approach, on the other hand, focuses on sampling multiple realizations, sometimes within a Bayesian setting (Aydin and Caers, 2017; Cherpeau et al., 2010, 2012; Cherpeau and Caumon, 2015; Holden et al., 2003; de la Varga and Wellmann, 2016; Wellmann et al., 2017; Grose et al., 2018). In order to address uncertainty caused by the inaccuracy of input data sets, some researchers propose sampling input data sets from user-defined distributions and using the implicit potential field method to directly simulate

multiple realizations (Wellmann et al., 2010; Lindsay et al., 2012). This approach potentially ignores other sources of uncertainty, especially uncertainty between data locations (Aitken et al., 2013). In some fully stochastic approaches, usually geological structures (e.g., faults and horizons) are stochastically modeled in a consistent way enforced by specified rules (Holden et al., 2003; Cherpeau and Caumon, 2015). Recently, in order to account for prior information, uncertainty quantification of 3D geological structures using a Bayesian framework has emerged (Aydin and Caers, 2017; Cherpeau et al., 2012; de la Varga and Wellmann, 2016; Wellmann et al., 2017; Grose et al., 2018). The advantage of using a Bayesian framework is that the uncertainty can be reduced when new data or information becomes available, which is a logical way of reasoning (Scheidt et al., 2018). However, constraining the models with dense hard data within the Bayesian framework is still challenging.

In addition to the use of level sets in implicit modeling and uncertainty quantification in geosciences (Aydin and Caers, 2017; Cherpeau and Caumon, 2015; Mallet, 2014; Moreno and Aanonsen, 2011; Xie et al., 2011), sophisticated techniques have also been developed for generating and evolving implicit interfaces (curves and surfaces) in the fields of computer graphics and computer vision (Osher and Fedkiw, 2002). In particular, dynamic level set methods, first proposed in Osher and Sethian (1988), are a relatively simple yet powerful way to implicitly represent and dynamically evolve complex interfaces. Algorithms have been developed to reconstruct implicit interfaces based on optimization (Juan et al., 2006; Zhao et al., 2001), or to sample posterior interfaces (mostly curves) using Markov chain Monte Carlo (McMC) (Fan et al., 2007; Iglesias et al., 2016). However, few if any applications for assessing the uncertainty of complex surfaces with dynamic level set methods have been reported in the literature to the best of our knowledge.

In this paper, we propose a new idea to incorporate stochastic motion with the level set methodology for assessing and visualizing the uncertainty of geological surfaces. Considering sampling the realizations of geological surfaces in a time sequence, we make the simple link that a surface that is unknown, except where the hard data is located, can still "move" (assuming the measurement error in the data is negligible). In that sense, we create stochastic motion of the surfaces, resulting in a "movie" of the surfaces. This idea is integrated with level set methods. With the level set methods, independent complex geological surfaces can be directly sampled by Monte Carlo and used for uncertainty assessment. Dependent realizations of geological surfaces are sampled by McMC and used to create a smooth movie to visualize the uncertainty, thereby potentially increasing people's comprehension of where and how large the spatial uncertainty is (Ehlschlaeger et al., 1997).

The paper is structured as follows. First, the methodology is presented in Section 2. Then, in Section 3, several 3D examples are provided to illustrate the method with different parameters. Next, an application of multi-lithology simulation constrained by dense drill-hole data and a clear geological age relationship is shown in Section 4, along with the associated uncertainty analysis.
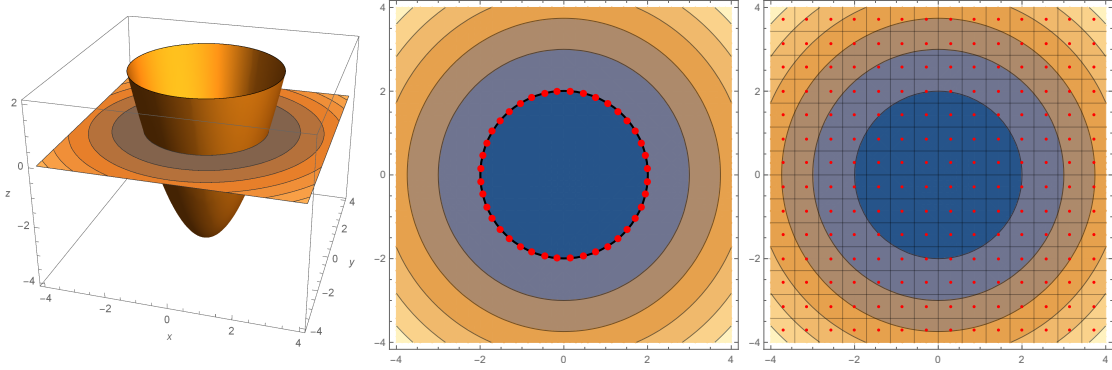
Figure 1: Level sets represent surfaces implicitly as isocontours of higher-dimensional functions, in contrast to explicit surface methods. Here we compare the representations for the 2D circle $x^2 + y^2 = 4$. (Left) The zero contour of the level set paraboloid $z = x^2 + y^2 - 4$ is the desired circle (several contours in the $z = 0$ plane are drawn, with different colors indicating regions between contours). (Middle) An explicit (also called Lagrangian) representation of the circle is a collection of points (red) and edges (thick black). (Right) Computationally, discrete samples (red) of the level set are stored in a uniform grid data structure; interpolation of these values is used to identify a desired contour.

Finally, Section 5 discusses the CPU runtime, and Section 6 concludes the paper. Produced movies for all examples in Section 3 and Section 4 can be found at: https://github.com/SCRFpublic/LevelSetMovies.

2. Methodology

Our methodology for assessing and visualizing uncertainty involves applying stochastic velocity fields to level set representations of geological surfaces, and constraining this motion to data and geological rules. We will therefore review the level set method first and then show how this can be used to represent and initialize surfaces. Finally, the notion of stochastic motion is explained.

2.1. Level Set Methods

With the level set method, an n-dimensional interface Γ (e.g., a curve in 2D, or a surface in 3D) is represented as the isocontour $\phi(\vec{x}) = c$ of an $(n + 1)$-dimensional function $\phi(\vec{x})$ called a level set function. This implicit approach fundamentally differs from explicit surface modeling (see Figure 1). Varying the chosen isocontour allows exploration of a family of geometries related by the geometry of the underlying level set. In particular, if the underlying level set is constrained to be a signed distance function (SDF), i.e., satisfying the special case $|\nabla \phi| = 1$ of the Eikonal equation, then several useful properties emerge. In this case, for an implicitly represented interface Γ, points satisfying $\phi(\vec{x}) < 0$ are inside Γ, points satisfying $\phi(\vec{x}) > 0$ are outside Γ, and points satisfying $\phi(\vec{x}) = 0$ lie exactly on Γ; moreover, for any point, $\phi(\vec{x})$ gives the signed distance to the nearest
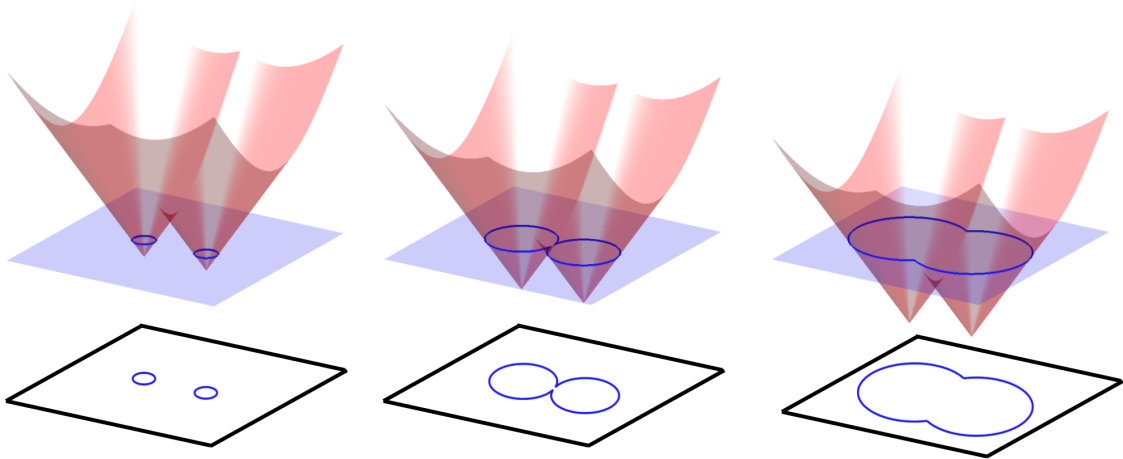
Figure 2: Different isocontours (blue) of a level set function (red) result in different interfaces (blue lines). The implicit nature of level sets makes it natural to perform topological operations like merging simply by shifting level sets or, with multiple level sets, via operations such as $\min(\phi_1, \phi_2)$ (union) or $\max(\phi_1, \phi_2)$ (intersection). (Source: (Gibou et al., 2018))

point on the surface, useful for many algorithms. Interfaces represented with level sets naturally support topological changes, such as merging and splitting, that are often challenging operations with explicit representations (see Figure 2).

Level set methods often dynamically evolve level sets by parameterizing them in time, $\phi(\vec{x}, t)$, and solving the "level set equation,"

$$\frac{\partial \phi(\vec{x}, t)}{\partial t} + \vec{v}(\vec{x}, t) \cdot \nabla \phi(\vec{x}, t) = 0. \tag{1}$$

The level set equation advects $\phi(\vec{x}, t)$ according to an n-dimensional velocity field $\vec{v}(\vec{x}, t)$, which in 3D we parameterize as (v_x, v_y, v_z). Since only the component of velocity in the normal direction has an effect on the level set equation, Equation 1 is equivalent to:

$$\frac{\partial \phi(\vec{x}, t)}{\partial t} + \vec{v}_n(\vec{x}, t) \cdot |\nabla \phi(\vec{x}, t)| = 0, \tag{2}$$

where $\vec{v}_n(\vec{x}, t)$ is the normal velocity. Temporally discretizing Equation 2 with the forward Euler method yields

$$\frac{\phi(\vec{x}, t + \Delta t) - \phi(\vec{x}, t)}{\Delta t} + \vec{v}_n(\vec{x}, t) \cdot |\nabla \phi(\vec{x}, t)| = 0. \tag{3}$$

Finally, we note that using the level set method allows certain geometric quantities to be easily computed; for example, the normal $\vec{N}$ to and mean curvature κ of a surface are given by

$$\vec{N} = \frac{\nabla \phi}{|\nabla \phi|}, \qquad \kappa = \nabla \cdot \vec{N}. \tag{4}$$

We use the open-source library PhysBAM[1] for representing and manipulating level sets.

---

[1] See http://physbam.stanford.edu.

2.2. Definition of the Stochastic Model

Let $C(\vec{x}, t)$ be a signed distance function that represents an implicit conceptual model of a geological surface, and $R(\vec{x}, t)$ denote a residual function that represents correlated variation made on that implicit conceptual model, at time t. We define a geological surface's corresponding level set function at time t, $\phi(\vec{x}, t)$, as the sum of $C(\vec{x}, t)$ and $R(\vec{x}, t)$, i.e.,

$$\phi(\vec{x}, t) = C(\vec{x}, t) + R(\vec{x}, t). \tag{5}$$

Equation 5 has similarities to the usual geostatistical assumption in random function theory of a mean plus a residual component (e.g. universal kriging) (Chilès and Delfiner, 2012; Kyriakidis and Journel, 1999). This formulation has also been applied in the uncertainty assessment of geological surfaces (Cherpeau et al., 2010; Cherpeau and Caumon, 2015). However, here we suggest the use of a random mean function, and not an unknown deterministic trend or mean function. The stochastic mean is useful, for example, if some initial 3D surface model $\phi_0(\vec{x})$ has been built that is too smooth and hence cannot be used as an implicit conceptual model. Note that this approach has similarities with a Bayesian geostatistical approach (Omre, 1999). To model a random implicit conceptual model, we use

$$C(\vec{x}, t) = \phi_0(\vec{x}) + R_C(\vec{x}, t), \tag{6}$$

where $R_C(\vec{x}, t)$ is another residual implicit random function, possibly with less variation than $R(\vec{x}, t)$. One may of course opt for the (non-Bayesian) traditional model, i.e., $C(\vec{x}, t) = \phi_0(\vec{x})$.

2.3. Level Set Implementation of the Stochastic Model

To implement the representation of Equation 5 in the level set formalism, we set $C(\vec{x}) = \phi(\vec{x}, t - \Delta t)$ and $R(\vec{x}, t) = |\vec{v}_n(\vec{x}, t - \Delta t)| \cdot \Delta t$ in Equation 5, which gives the following level set equation:

$$\phi(\vec{x}, t) = \phi(\vec{x}, t - \Delta t) + |\vec{v}_n(\vec{x}, t - \Delta t)| \cdot \Delta t, \tag{7}$$

where Δt is always set to 1. To obtain $|\vec{v}_n(\vec{x}, t - \Delta t)|$, at first, a Gaussian realization is defined on the surface $C(\vec{x}, t) = 0$. This is achieved by creating a Gaussian realization for the entire grid and extracting the values on the mean surface, which themselves are also Gaussian. Then the values on the mean surface are extrapolated in the normal direction (Figure 3), called "velocity extension" (Adalsteinsson and Sethian, 1999), meaning we are creating velocities that satisfy:

$$\nabla|\vec{v}_n(\vec{x}, t)| \cdot \nabla\phi(\vec{x}, t) = 0. \tag{8}$$

Velocity extension can be implemented by:

$$\vec{v}_n(\vec{x}, t) = \vec{v}_n\left(\vec{x} - \phi(\vec{x}, t) \cdot \vec{N}, t\right). \tag{9}$$
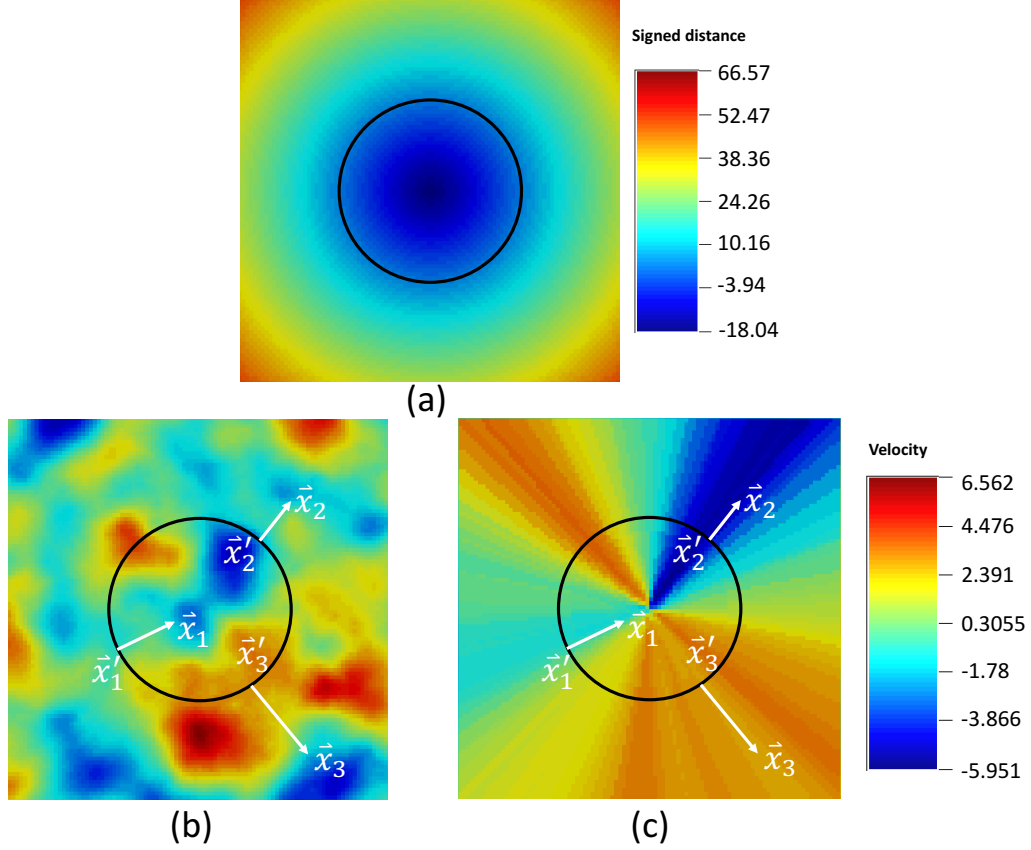
Figure 3: Illustration of velocity extension. (a) shows a sphere (black circle) defined by its signed distance function $\phi(\vec{x})$. (b) shows a Gaussian realization for the entire grid. (c) shows the extended velocity field. Values (velocities) on the sphere are extracted and extended in the normal direction. For instance, the velocities at locations $\vec{x}_1$, $\vec{x}_2$ and $\vec{x}_3$ are equal to the velocities at $\vec{x}_1' = \vec{x}_1 - \phi(x_1)\vec{N}$, $\vec{x}_2' = \vec{x}_2 - \phi(x_2)\vec{N}$ and $\vec{x}_3' = \vec{x}_3 - \phi(x_3)\vec{N}$.

$R_C(\vec{x}, t)$ in Equation 6 can also be created by this velocity extension implementation. In contrast to directly adding a Gaussian random field to an initial level set function, such as in Cherpeau et al. (2010) and Cherpeau and Caumon (2015), velocity extension perturbs all isocontours consistently in order to avoid creating unexpected isolated objects distant from the base surface $C(\vec{x}, t) = 0$ (see Figure 4 for an example). Velocity extension is useful since it ensures that $\phi(\vec{x}, t)$ remains a SDF during evolution (Adalsteinsson and Sethian, 1999). The SDF properties are hence preserved, without ad-hoc modifications. Additionally, the velocity extension will be useful to create a random walk of the surface that has microscopic reversibility (Fan et al., 2007).

2.4. Construction of the Implicit Conceptual Model

To construct an implicit conceptual model, we need to initialize the signed distance function $\phi_0(\vec{x})$ in Equation 6. In some applications, analytic functions with uncertain parameters are enough
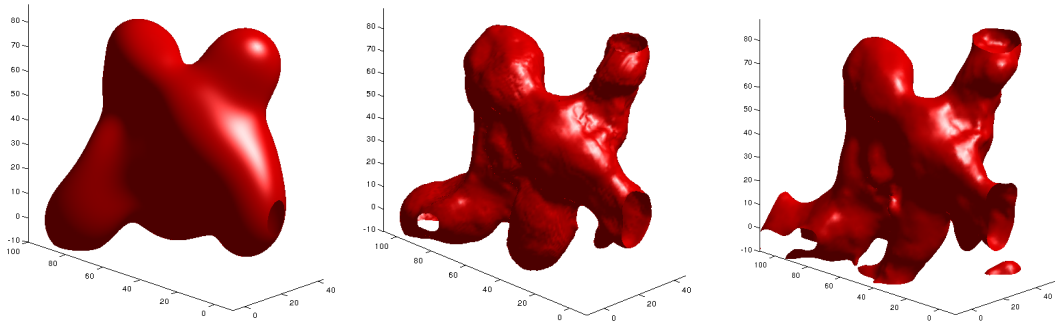
Figure 4: Comparison of the results of using velocity extension (middle) and directly adding a Gaussian random field (right) to the implicit function of a base surface (left). The same Gaussian realization is used for both methods in the test.

to initialize simple shapes such as planes, ellipsoids and channels. In complex applications, more sophisticated approaches are required to initialize an implicit surface model. Data constraints are often placed on the generation of surface models. One efficient way to initialize the signed distance function is the surface reconstruction method proposed by Zhao et al. (2001). Zhao et al. (2001) reconstructs an interface Γ from data points by first initializing Γ to be a rough initial guess of the final surface (for instance, a bounding box such as the grid itself that encloses all the data points. The fast tagging method described in (Zhao et al., 2001) is then applied, which iteratively excludes from Γ points that are outside a radius of any data points. The fast tagging method runs in $O(N \log N)$, where N is the number of grid cells bounded by the initial guess for Γ. Finally, to obtain a smoother representation of Γ, the convection equation

$$\frac{d\Gamma}{dt} = -\nabla d\left(\vec{x}\right) \tag{10}$$

is integrated for several (fictitious) time steps, where $d\left(\vec{x}\right)$ is the distance from a point $\vec{x}$ to the nearest data point. Thus, Γ is attracted towards the data set, creating a "shrink-wrapped" level set surface that matches the data. The initialization procedure is illustrated in Figure 5. After initialization, the conceptual models are constructed by Equation 6 and have larger variability than simply using ϕ_0.

2.5. Multiple Level Sets

For representing multi-category geological surfaces, each category uses an independent level set function. Often, a geological age relationship constraint is necessary when a prior age relationship is known for multiple objects, such as stratigraphies, faults, and lithologies (Cherpeau et al. (2010). The geological age relationship can be expressed by the difference operation of level sets (Museth et al., 2003): consider a binary case with categories A and B, if category A is older than category
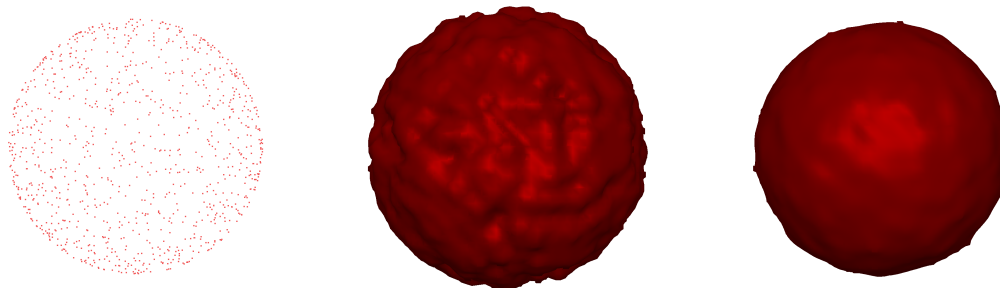
8

Figure 5: Illustrates the surface reconstruction process of (Zhao et al., 2001), which we use for initial model generation. (Left) We randomly sample $1,000$ points from the surface of a 3D sphere of radius 10 centered at the center of the 100^3 domain, a uniform Cartesian grid with resolution $\Delta x = 0.5$. The initial guess for a surface that fits these points is a box that fills the entire domain (i.e., the grid itself). (Middle) The fast tagging method efficiently refines the initial guess to a coarse approximation of a surface. (Right) After 30 steps of convection, the reconstructed surface appears quite smooth. The surface is not perfectly spherical due to the sparsity of the input points and the limited grid resolution (there is inherent $O(\Delta x)$ error in the final result).

B, then $\phi(A) = \min(\phi(A), -\phi(B))$, and $\phi(B) = \phi(B)$; otherwise, $\phi(A) = \phi(A)$, and $\phi(B) = \min(\phi(B), -\phi(A))$. In order to enforce the geological age relationship, multiple level sets are independently initialized for each object at first (see Figure 6). The initial model should reflect the initial geological states, meaning that the older level sets are not truncated by newer level sets yet. Then, the difference operation is applied to the level sets according to the geological age relationship.

2.6. Stochastic Motion by Monte Carlo and McMC

For assessing and visualizing the uncertainty, stochastic motion is defined for geological surfaces, in the sense that both the implicit conceptual model and the residual function change with time. Two sampling approaches, Monte Carlo and McMC, are proposed to draw independent and dependent realizations, respectively.

2.6.1. Monte Carlo

In the Monte Carlo sampling, a new realization of the implicit conceptual model and a new realization of the residual function are drawn at every new time t independently. Hence the time t is simply a counter for realizations. For conditional simulation, we first set the values of conditioning data points to zero and then draw conditional Gaussian realizations, so that the geological surfaces do not move away from the conditioning data.
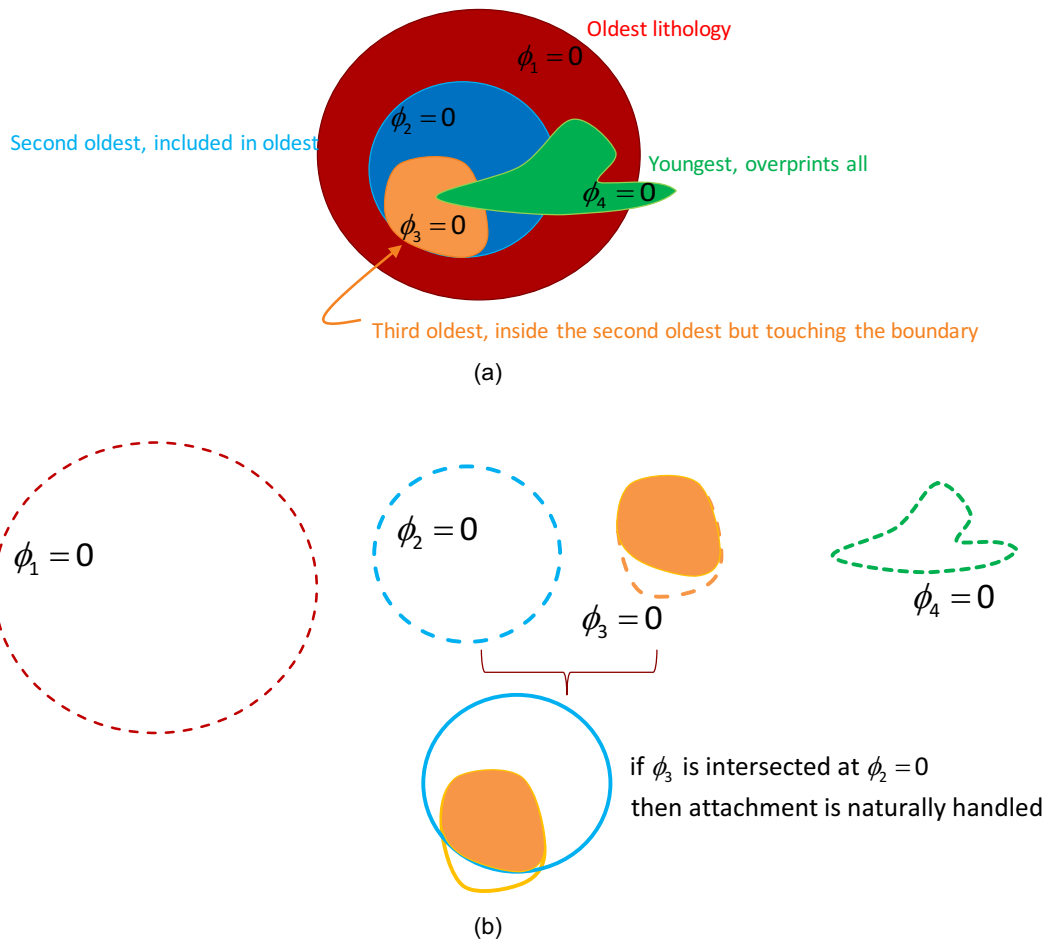
Oldest lithology
$\phi_1 = 0$

$\phi_2 = 0$

Second oldest, included in oldest

Youngest, overprints all

$\phi_4 = 0$

$\phi_3 = 0$

Third oldest, inside the second oldest but touching the boundary

(a)

$\phi_1 = 0$

$\phi_2 = 0$

$\phi_3 = 0$

$\phi_4 = 0$

if ϕ_3 is intersected at $\phi_2 = 0$
then attachment is naturally handled

(b)

Figure 6: A geological age relationship example. (a) Four level sets are used to represent four lithologies, which have an age relationship indicated in the figure; (b) Independent initialization of each level set without truncation.
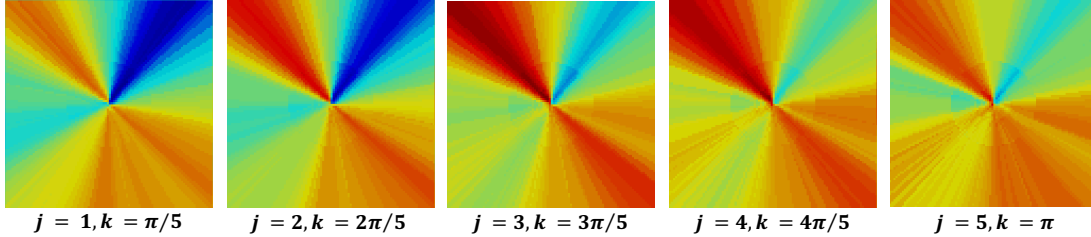
$$j = 1, k = \pi/5 \qquad j = 2, k = 2\pi/5 \qquad j = 3, k = 3\pi/5 \qquad j = 4, k = 4\pi/5 \qquad j = 5, k = \pi$$

Figure 7: Illustration of the gradual deformation of the residual function. The residual function is a normal extension of the Gaussian realization defined on the sphere in Figure 3.

2.6.2. Markov chain Monte Carlo (McMC)

We can also define a McMC sampling of the uncertainty of geological surfaces. McMC can be useful when needing to condition to more complex data that require the definition of a likelihood function. In this paper, however, we focus on using McMC for drawing from the same distribution as with Monte Carlo, meaning drawing from a prior distribution. We propose to use the gradual deformation method (GDM) (Hu, 2000), as a McMC method for sampling the surfaces. Note that we do not use GDM in the classical sense as an optimizer. Instead, our approach uses GDM to generate a random walk in the prior space. For this random walk to converge to a stationary distribution, the Markov chain generated by GDM needs to have detailed balance (microscopic reversibility) (Green, 1995; Medhi, 1994; Mosegaard and Sambridge, 2002). In other words, the probabilities of going from $\phi(\vec{x}, t)$ to $\phi(\vec{x}, t + \Delta t)$ needs to be the same as the probability of going from $\phi(\vec{x}, t + \Delta t)$ to $\phi(\vec{x}, t)$. The time t is now equivalent to the iteration in the chain. A proof that shows GDM provides a random walk in the prior space is given in the Appendix. Additionally, defining the gradual deformation on the velocity extension, allows for the SDF properties to be preserved during the random walk.

McMC can then be used to visualize the uncertainty as a continuously evolving "movie" of the geological surfaces it generates. Because of the properties shown in Appendix, this movie has equivalent uncertainty as Monte Carlo sampling. Figure 7 shows the gradual change of a residual function $R(\vec{x}, t)$.

3. Illustration Cases

This section illustrates the method, studies the influence of parameters, demonstrates uncertainty assessment, and analyzes important output statistics, using a synthetic 3D setting with a grid size of $100 \times 100 \times 100$. In order to show how the method works for diverse surface types, the initial surfaces are three objects generated by three analytic functions: a plane, a sphere and a cosine-type wave (see Figure 8). The plane and the wave are open surfaces and the sphere is a closed body. To investigate the uncertainty affected by conditioning data, three drill-holes are used

as conditioning data, and they pass through the plane and wave. A synthetic age relationship is assigned to three objects, so that the plane is truncated by the other two objects and the wave truncates the other two. The Gaussian realizations for defining the mean function and the residual function are created using sequential Gaussian simulation (SGS) with mean zero (Chilès and Delfiner, 2012; Remy et al., 2009). A Gaussian variogram model is used in all of our tests. Other variogram models, such as an exponential variogram, could also be used, but they could create noisier surfaces that may be less geologically plausible than a Gaussian model. For comparing the influence of parameters, three series of conditional Gaussian realizations are generated, each series containing 100 realizations with sill 5 and range 20, sill 5 and range 60, and sill 10 and range 20, respectively (Figure 8). These parameters have the same unit as the grid size. One series of unconditional Gaussian realizations with sill 5 and range 20 is also generated as a comparison. McMC by GDM is used to create a smooth movie and each GDM cycle contains 10 deformation steps.

3.1. Simulation Results and Uncertainty Assessment

The simulation results are compared and the uncertainty is assessed in this section. Two realizations from the movie are selected and shown in the first and the second columns of Figure 9. Notice how the sill and range contribute to the variability of the surfaces. The surfaces separate the space into three domains (see the third column of Figure 9 for the sections of the domains with the truncation rule enforced). One quantitative way of assessing the uncertainty of 3D surfaces is using the information entropy (Shannon, 1948) and has been applied in geoscience as a quality measurement of geological models (Wellmann and Regenauer-Lieb, 2012). As in Wellmann and Regenauer-Lieb (2012), we consider that every surface separates the grid into two sub-domains so the uncertainty of the surfaces is simply represented by the entropy of every grid cell. Only the independent geological surfaces sampled by Monte Carlo, (i.e., the first realization of every GDM cycle) are retained to calculate the entropy. The last column of Figure 9 shows entropy maps of the stochastic motion. In the entropy maps, the blue color indicates zero entropy (i.e., certainty), and other colors form a "color band" that mirrors possible locations of surfaces. The width of the "color band" reflects the variance of the Gaussian realization (i.e., the sill of the variogram). The larger the variance is, the wider the "color band" is. Conditioning is also shown by the entropy maps: the entropy values are zero on the drillholes and small near drillholes. The entropy map of the unconditional stochastic motion in the last row is shown for comparison. Most uncertainty lies in areas where multiple surfaces have a high possibility intersecting each other (see the orange and red regions in Figure 9).

3.2. Output Statistics: Volume and Surface Roughness

This section shows how the parameters affect some important output statistics of a geological structure model, such as the volume and surface roughness (Mallet, 2014; Thore et al., 2002). We
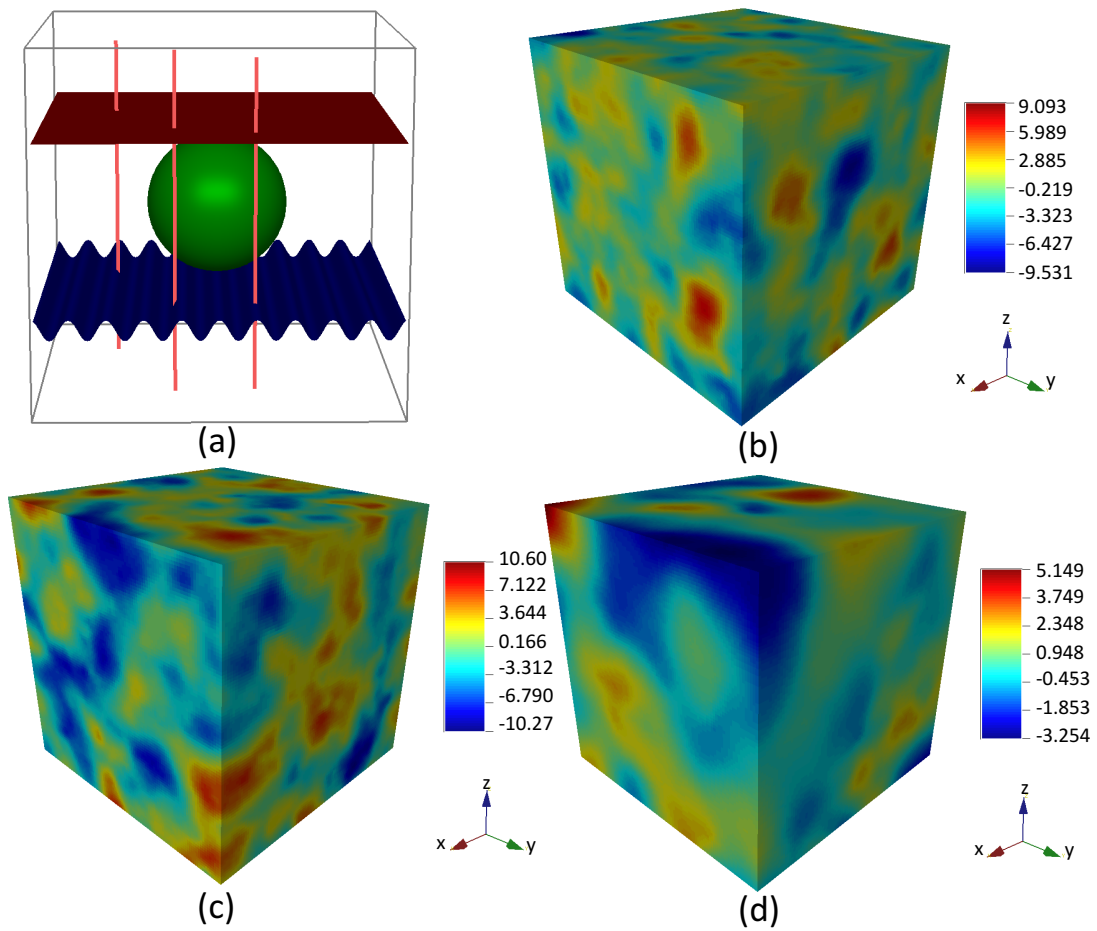
Figure 8: Initial surfaces and velocity fields. (a) The initial three objects and three drill-holes are visualized together. Realizations of velocities are generated using three boreholes as conditioning data. Three realizations generated with (b) sill 5 and range 20, (c) sill 10 and range 20, and (d) sill 5 and range 60 are shown. The colors in the realizations represent the velocity magnitudes.
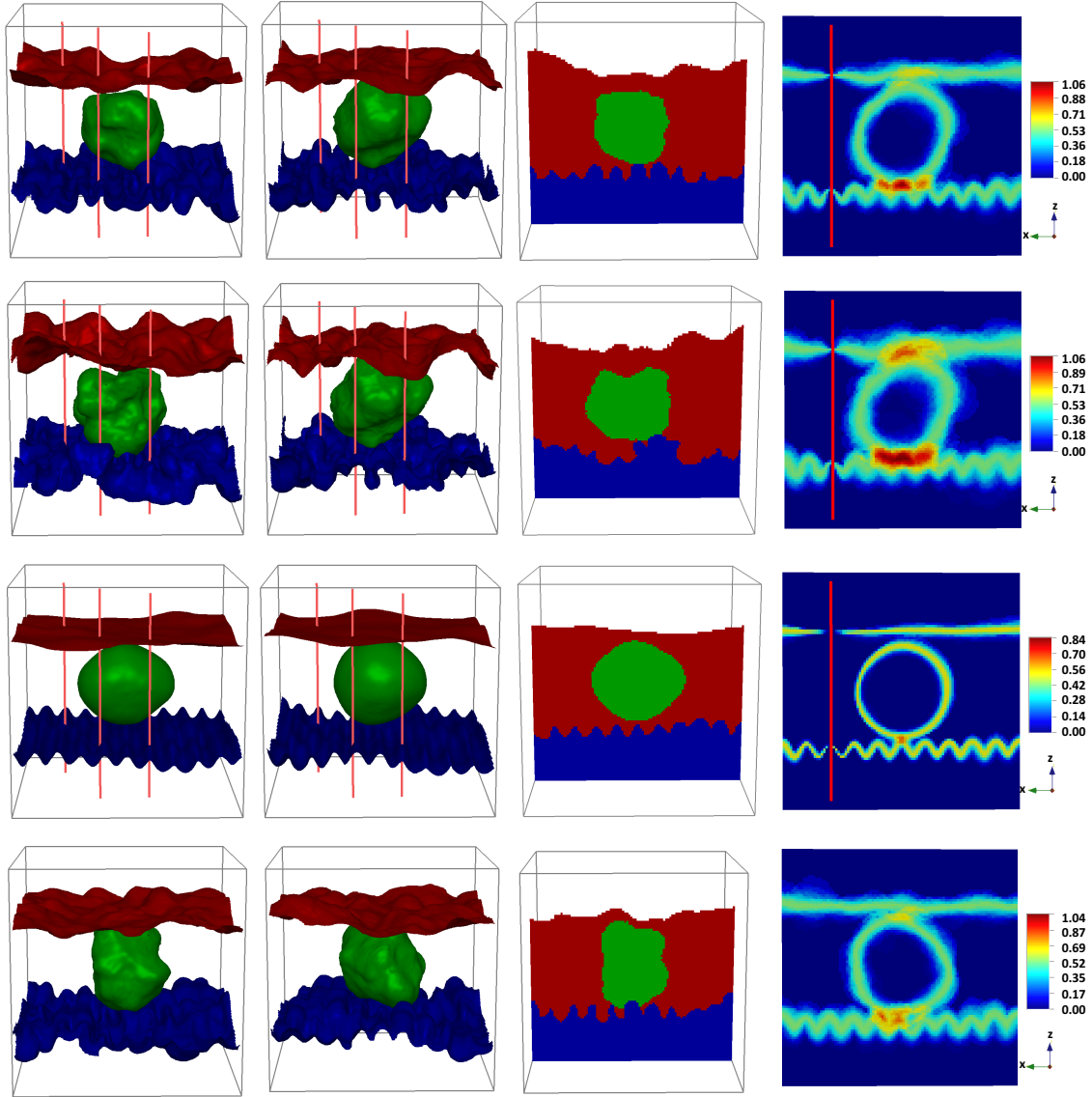
Figure 9: Snapshots of surfaces at time 60 (first column) and at time 90 (second column), sections of geological domains (third column) and the entropy maps (fourth column). The first three rows are the results of the conditional stochastic motion with sill 5 and range 20, sill 10 and range 20, and sill 5 and range 60, from top to bottom. The last row shows the results of the unconditional stochastic motion with sill 5 and range 20.
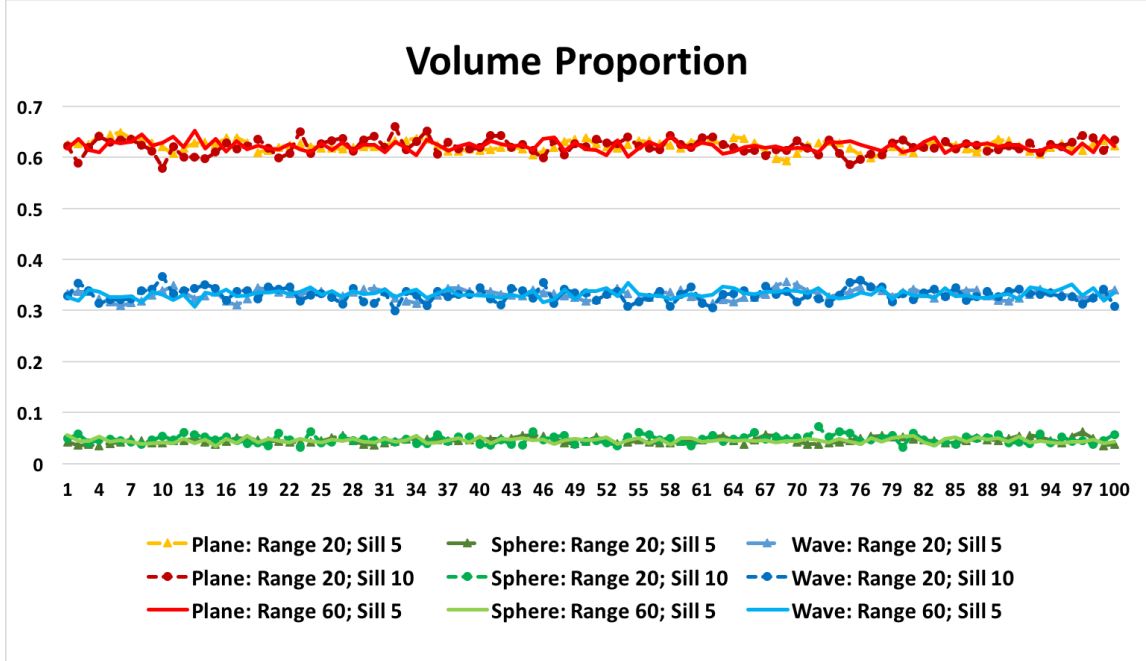
Figure 10: The change of volume proportion with three parameter settings. The horizontal axis shows time steps and the vertical axis shows the volume proportion of the domains separated by three surfaces.

calculate the volumes of the three domains separated by surfaces (see the third column in Figure 9 for the sections of the domains). Figure 10 shows the change of volume proportion during the conditional stochastic motion with three parameter settings. It is shown that the initial volumes are maintained for all cases. The effect of maintaining the volume is in fact due to that the stationary isotropic Gaussian realizations are used, which are divergence-free (Rogers and Williams, 2000). A divergence-free velocity field is the condition for the conservation of mass (or volume if the density is constant) in continuum mechanics (Osher and Fedkiw, 2002). However, it should be noted that if the size of the mean surface is so small that the Gaussian realization is not stationary on the mean surface, the volume may no longer be maintained.

Figure 9 suggests the surfaces are visually "rougher" with larger sills and smaller ranges. This observation coincides with the consequence of geostatistical simulation where larger sills and smaller ranges result in more variability in realizations. In order to quantitatively compare the surface roughness, the variance of the mean curvature: $Variance(\kappa)$ is used as the global indicator of surface roughness. $Variance(\kappa)$ of the three parameter settings in Section 3.1 are compared in Figure 11. Figure 11 shows a comparison of resulting $Variance(\kappa)$ with respect to time step for the three parameter settings. The plots suggest that the surface roughness is related to the roughness of the mean surface, the sill and the range. Although some variations exist, there is a general trend of roughness decrease when increasing the range, or decreasing the sill.
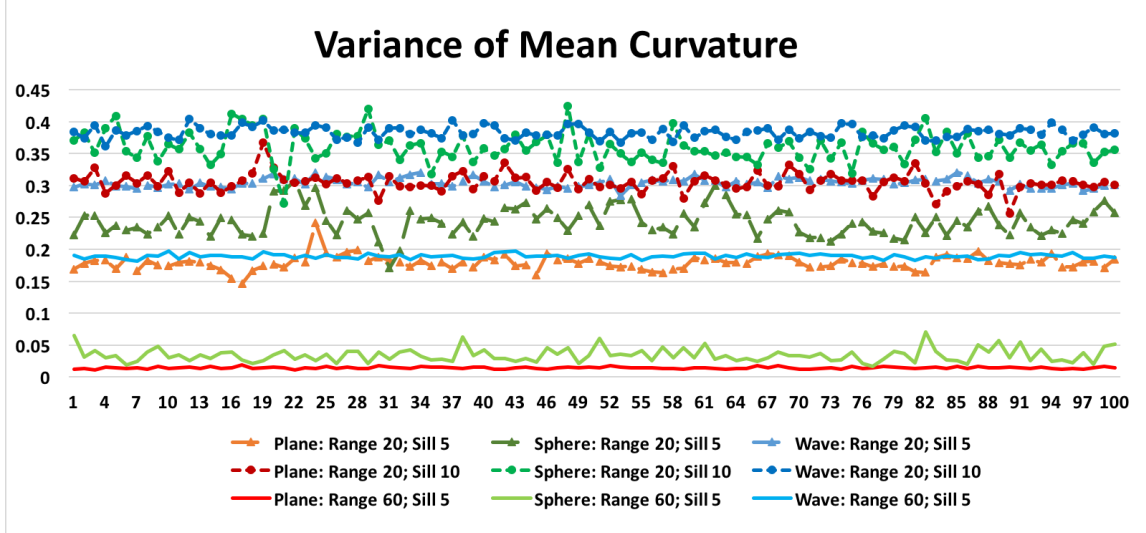
15

Figure 11: The change of variance of mean curvature (vertical axis) w.r.t. time step (horizontal axis) with three parameter settings.

4. Case Study: Synthetic Copper Deposit

4.1. Data Description

To evaluate the method's performance in a more realistic setting where surfaces' geometry and topology are complex, and constrained by dense hard data and a clear geological age relationship, we apply our methodology with a synthetic data set motivated by a real copper deposit. In this case, approximately 50 drillholes are used as hard constraints, indicating seven lithologies (Figure 12). An interpreted model was built, constrained by these drillholes and geologists' understanding of the geological age relationship in this case (Figure 12) (this model was given as is, hence one can consider it as a smooth deterministic interpretation of the actual variability). The lithologies are named by their age hierarchy, so *Lithology* 1 ⊇ *Lithology* 2 ⊇ *Lithology* 3 ⊇ ... ⊇ *Lithology* 7. The older lithologies are truncated by younger lithologies. Although the geological age relationship is known and fixed, the geometry and topology of each lithology are uncertain. Drillholes are dense in the center and at the top, but are sparse at the bottom and near the boundary of the grid.

4.2. Simulation

For sampling surfaces and maintaining the assumed geological age relationships, we use an interpreted model to initialize the level sets with the fast tagging method and convection equation (Equation 10) and get $\phi_0(\vec{x})$. To simulate, implicit conceptual models and residuals, i.e., $\phi_0 + R_C$ and R, are sampled by both Monte Carlo and McMC to generate geological surfaces. In order to maintain the age relationship during stochastic motion, we use the same truncation rule at all time steps. The simulation grid size is $120 \times 120 \times 100$. Since no additional information on
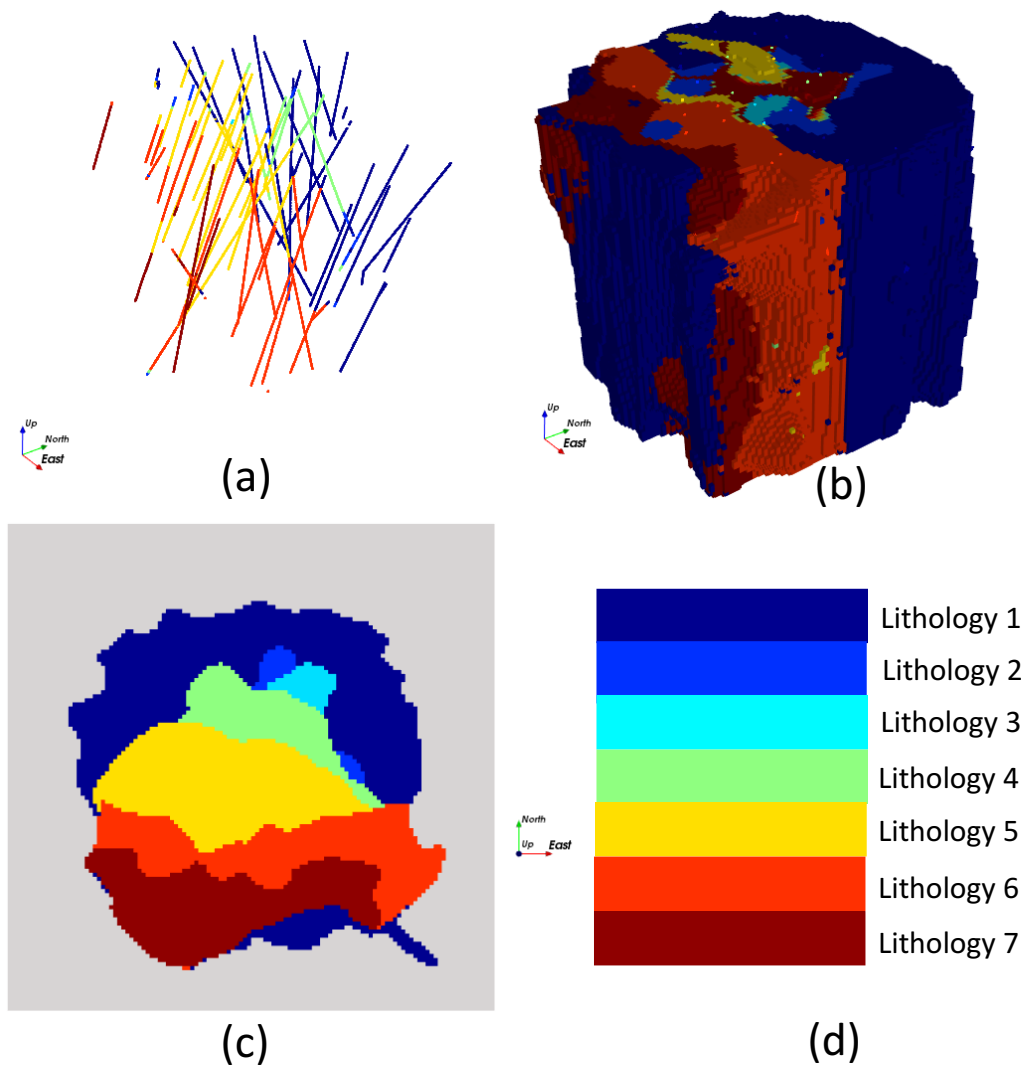
Figure 12: Synthetic copper data set. (a) shows 50 drillholes. (b) shows an interpreted model of the area. The interpreted model shows a complex shape. (c) a section view of the interpreted model. (d) shows the geological age relationship (old to young from the top to the bottom). Seven colors in (d) correspond to seven lithologies in the data.

surface roughness was made available to us for this virtual case, we used an arbitrary variogram for R_C and R with sill 10 and range 10 (same unit as the grid size). The output movies show a gradual change in the geometry and topology (see accompanied movies in https://github.com/SCRFpublic/LevelSetMovies). Figure 13 (a) and (b) show two copper deposit realizations drawn with Monte Carlo. One can observe their differences in the geometry and topology. The sections (Figure 13 (c) and (d)) indicate that the geological age relationship is maintained during the stochastic motion. Figure 13 (e) and (f) show the change of surface connectivity between two different realizations. It is clear that the two realizations have different connectivity compared to Figure 12(c). Because of the higher density of drill-holes, the surface variability is smaller in the center area and at the top, comparing to the bottom area. The probability that any spatial location belongs to *Lithology* 4 is shown in Figure 14 (a). It is shown that the probabilities are large near data points that indicate *Lithology* 4, and are small away from those points. The entropy of all surfaces is shown in Figure 14 (b). Notice that larger entropies are seen at the bottom, because of the sparsity of drillholes.

5. CPU runtime

In terms of the method's runtime, we discuss the runtime per time step of the stochastic motion, referred to as the "unit runtime," and the runtime for a movie with 100 time steps, plus the initialization time, referred to as the "total runtime." The number of level sets and the grid resolution are dominating factors for the unit runtime. Most of the computation time is spent on creating the Gaussian realizations and extending the velocity in the normal direction. We initialize the surfaces and create all the Gaussian realizations at the beginning. After that, the unit runtime is linear in the number of level sets since we update each level set independently. Table 1 lists both the unit runtime and total runtime for the two cases in Section 3 and 4. All simulations are run on a laptop with a Intel Core i7-7700HQ CPU with a frequency of 2.80GHz. We note that on a single CPU core, the present method's efficiency is promising; moreover, much of our algorithm could be easily parallelized in order to improve performance since each level set is treated independently.

Table 1: Runtimes for the 3D object example and the copper case

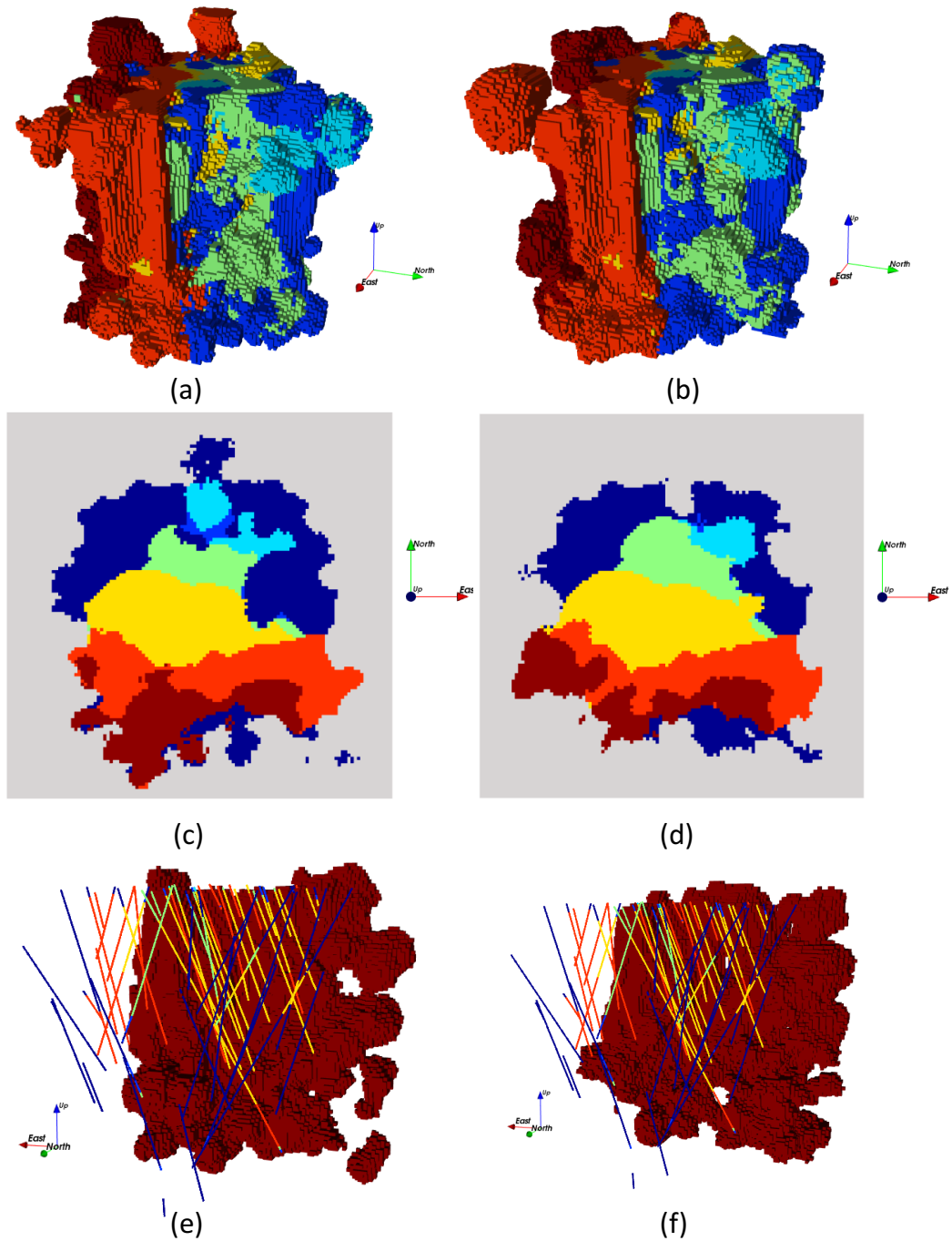| Cases	Unit runtime (1 time step)	Total runtime (initialization + 100 time steps)
Illustration case	3.9s	407.3s
Synthetic copper case	19.4s	1994.5s

18

Figure 13: Realizations of the synthetic copper case. (a) and (b) are two realizations from the stochastic motion (*Lithology* 1 is made transparent). (c) and (d) are sections of the models that show the geological age relationship. (e) and (f) are two realizations of *Lithology* 7. Note that all figures use the same color scheme as Figure 12 (d).
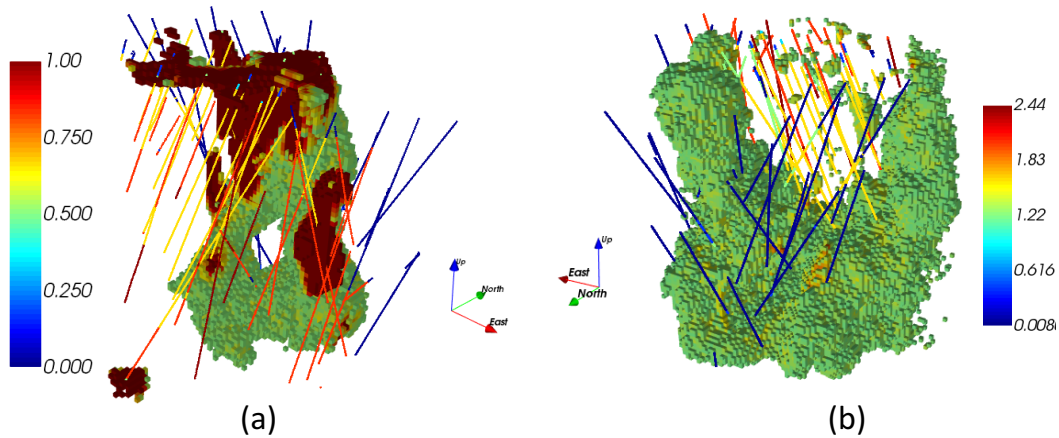
Figure 14: Probability and entropy maps. (a) is the probability that any location belongs to *Lithology* 4 (probabilities below 0.4 are made transparent). (b) is the entropy of all surfaces (entropies below 1.2 are made transparent).

6. Conclusion

In this paper, we propose a new methodology for assessing and visualizing the uncertainty of 3D geological surface models using level sets by the means of stochastic motion. The method takes advantage of the level set methods and directly simulates geological surfaces with complex geometries and topologies, subject to data and geological age relationship constraints. Monte Carlo sampling of independent realizations are retained for assessing the uncertainty. Markov chain Monte Carlo sampling is used for generating a continuously evolving movie that may enhance people's perception of the uncertainty, as suggested by the growing body of work on building improved visualization systems for the geosciences as well as a recent survey showing the current difficulty of communicating uncertainty for mineral resource geologists (see Hyde et al. (2018) and the references therein). The uncertainty and output statistics such as the volume and surface roughness are related to the input parameters. The CPU runtime analysis shows the method is efficient enough for the presented cases. What is not yet treated in this paper is the specification of model parameters for both the mean and residual functions. Our future work will focus on developing a Bayesian inference framework that infers the parameters based on data. Moreover, we plan to extend to other types of objects, in particular, structural modeling of faults and folds. Level sets have been used to models these types of geometries, as indicated in the introduction; therefore, the method of stochastic motion can readily be applied to that setting.

With the same goal as other methods for stochastically simulating geological structures mentioned in the introduction, the method is mostly applicable to model objects or domains where

classical geostatistical approaches become difficult to apply (Chilès and Delfiner, 2012; Mariethoz and Caers, 2015). In real field applications, it will complement geostatistical methods by creating the domain wherein the more classical approaches can proceed; often the geometry and topology of these domains are the zero-th order uncertainty in practical applications (Jones et al., 2013; Mallet, 2014; Thore et al., 2002).

Acknowledgements

Appendix: Gradual deformation as a Markov chain Monte Carlo sampler

In Hu et al (2000), gradual deformation was proposed to solve non-linear inverse problems with Gaussian prior distributions. The main idea is to write a Gaussian realization $v(t)$ as a linear combination of two independent Gaussian realizations v_k and v_{k+1}, i.e.,

$$v(t) = \sin(t) \cdot v_k + \cos(t) \cdot v_{k+1}. \tag{11}$$

Then, a two-loop optimization on both k (outer loop) and t (inner loop) is used to optimize an objective function (difference between data and simulated data), constrained to the stated Gaussian prior. Multiple solutions are obtained by starting from different initial samples. As pointed out in Hansen et al. (2012), this form of sampling is not a Markov chain Monte Carlo since the method is dependent on the optimization algorithm and hence on the initial model. As a result, sampling from a posterior (or prior) is only approximate. Here, we suggest the use of the GDM in a completely different setting. Instead of optimizing, we use GDM to generate a Markov chain; we generate a chain of realizations by changing (not optimizing) k discretely and t using a time step Δt in Equation 11. In this appendix, we provide a proof that GDM is a Markov chain Monte Carlo method regardless of the time steps Δt. To do this, we need to show that gradual deformation has the property of detailed balance (microscopic reversibility, see Green (1995), Medhi (1994) and Mosegaard and Sambridge (2002)). In other words, when

$$P(v(t) \rightarrow v(t + \Delta t)) = P(v(t + \Delta t) \rightarrow v(t)). \tag{12}$$

If Equation 12 does not hold, then in order to adjust the balance, we need to add an acceptance/rejection step with a probability given by the ratio

$$\alpha = \frac{P(v(t) \rightarrow v(t + \Delta t))}{P(v(t + \Delta t) \rightarrow v(t))}. \tag{13}$$

To simplify notation, call $t = x$, $t + \Delta t = y$, $v_k = v_1$ and $v_{k+1} = v_2$. Then

$$v(x) = \sin(x) \cdot v_1 + \cos(x) \cdot v_2 \tag{14}$$

Then we have:

$$
\begin{aligned}
v(x + y) &= \sin(x + y) \cdot v_1 + \cos(x + y) \cdot v_2 \\
&= \sin(x) \cdot (\cos(y) \cdot v_1 - \sin(y) \cdot v_2) \\
&\quad + \cos(x) \cdot (\sin(y) \cdot v_1 + \cos(y) \cdot v_2) \\
&= \sin(x) \cdot v_1' + \cos(x) \cdot v_2'
\end{aligned}
\tag{15}
$$

Note that v_1' and v_2' are independent random variables. Similarly, going back from $x + y = z$ to x yields:

$$v(z) = \sin(z) \cdot v_1 + \cos(z) \cdot v_2 \tag{16}$$

Similarly to Equation 15, we have:

$$
\begin{aligned}
v(x) &= \sin(z - y) \cdot v_1 + \cos(z - y) \cdot v_2 \\
&= \sin(z) \cdot (\cos(y) \cdot v_1 + \sin(y) \cdot v_2) \\
&\quad + \cos(z) \cdot (-\sin(y) \cdot v_1 + \cos(y) \cdot v_2) \\
&= \sin(z) \cdot v_1'' + \cos(z) \cdot v_2''
\end{aligned}
\tag{17}
$$

Since distributions of all variables are Gaussian, detailed balance entails that both the conditional mean and variance are equal, i.e.,

$$E[v(x + y)|v(x)] = E[v(x)|v(x + y)] \tag{18}$$

and

$$Var[v(x + y)|v(x)] = Var[v(x)|v(x + y)] \tag{19}$$

In terms of conditional expectation this then entails that:

$$
\begin{aligned}
E[v_1'|v_1] &= E[v_1''|v_1] \\
E[v_2'|v_2] &= E[v_2''|v_2]
\end{aligned}
\tag{20}
$$

A simple calculation shows that

$$
\begin{aligned}
E[v_1'|v_1] &= E[v_1''|v_1] = \cos(y)v_1 \\
E[v_2'|v_2] &= E[v_2''|v_2] = \cos(y)v_2
\end{aligned}
\tag{21}
$$

Similarly, for the variance we get:

$$
\begin{aligned}
Var[v_1'|v_1] &= Var[v_1''|v_1] = \sin^2(y) \\
Var[v_2'|v_2] &= Var[v_2''|v_2] = \sin^2(y)
\end{aligned}
\tag{22}
$$

For small Δt, it is easy to show that using a Taylor expansion:

$$v(t + \Delta t) = v(t) + \Delta t \cdot (\cos(x)v_1 - \sin(x)v_2)$$
$$= v(t) + \Delta t \cdot v \tag{23}$$

In this case, detailed balance is trivial to show because of the addition of a random component with mean zero and standard deviation Δt. Caers (2007) showed with examples that gradual deformation leads to divergence when the size of the random vector is small relative to the number of perturbations made. This can now be understood as follows. Consider v to be a random vector with covariance matrix C. A simple way to generate samples of v is using Cholesky decomposition, meaning:

$$v = m + L^T v_0 \tag{24}$$

with v_0 is vector of independent Gaussian deviates and $C = L^T L$. Because the vector v_0 is of finite size, we have that $v_0^T v_0$ is not necessarily exactly equal to zero (spurious correlation). This also means that there is no detailed balance since for another sample v' we have $v_0'^T v_0'$, hence

$$P(v \to v') \sim \exp(-(v' - m)C^{-1}(v' - m)^T) = \exp(-v_0'^T v_0') \tag{25}$$

Likewise

$$P(v' \to v) \sim \exp(-(v - m)C^{-1}(v - m)^T) = \exp(-v_0^T v_0) \tag{26}$$

Hence GDM requires an acceptance/rejection probability of

$$\alpha = \exp(-v_0'^T v_0' + v_0^T v_0) \tag{27}$$

This probability is however close to 1 for high-dimensional problems, or problems where the sample size is orders of magnitude less than the dimension of the problem, which is the case for large spatial problems. The implications here for stochastic motion is that McMC is possible using GDM, and that the visualization, i.e. the "movie" of dependent realizations reflects the actual uncertainty sampled using Monte Carlo by independent realizations.

References

D. Adalsteinsson and J. A. Sethian. The fast construction of extension velocities in level set methods. *Journal of Computational Physics*, 148:2 – 22, 1999.

A. R. A. Aitken, E-J. Holden, and M. C. Dentith. Semiautomated quantification of the influence of data richness on confidence in the geologic interpretation of aeromagnetic maps. *GEOPHYSICS*, 78:J1 – J13, 2013.

Orhun Aydin and Jef Caers. Quantifying structural uncertainty on fault networks using a marked point process within a bayesian framework. *Tectonophysics*, 712–713:101 – 124, 2017.

Jef Caers. Comparing the gradual deformation with the probability perturbation method for solving inverse problems. *Mathematical Geology*, 39:27 – 52, 2007.

Jef Caers. *Modeling Uncertainty in the Earth Sciences*. Wiley-Blackwell, 2011.

P. Calcagno, J.P. Chilès, G. Courrioux, and A. Guillen. Geological modelling from field data and geological knowledge: Part i. modelling method coupling 3d potential-field interpolation and geological rules. *Physics of the Earth and Planetary Interiors*, 171:147 – 157, 2008.

Guillaume Caumon. Towards stochastic time-varying geological modeling. *Mathematical Geosciences*, 42:555 – 569, 2010.

Guillaume Caumon, Anne-Laure Tertois, and Ling Zhang. Elements for stochastic structural perturbation of stratigraphic models. In *Petroleum Geostatistics*, Cascais, Portugal, September 2007. EAGE.

Guillaume Caumon, Gary Gray, Christophe Antoine, and Marc-Olivier Titeux. Three-dimensional implicit stratigraphic model building from remote sensing data on tetrahedral meshes: Theory and application to a regional model of la popa basin, ne mexico. *IEEE Transactions on Geoscience and Remote Sensing*, 51:1613 – 1621, 2013.

Nicolas Cherpeau and Guillaume Caumon. Stochastic structural modelling in sparse data situations. *Petroleum Geoscience*, 21:233 – 247, 2015.

Nicolas Cherpeau, Guillaum Caumon, and Bruno Lévy. Stochastic simulations of fault networks in 3d structural modeling. *Comptes Rendus Geoscience*, 342:687 – 694, 2010.

Nicolas Cherpeau, Guillaume Caumon, Jef Caers, and Bruno Lévy. Method for stochastic inverse modeling of fault geometry and connectivity using flow data. *Mathematical geosciences*, 44:147 – 168, 2012.

J P Chilès, C Aug, A Guillen, and T Lees. Modelling the geometry of geological units and its uncertainty in 3d from structure data: the potential-field method. In *Orebody modelling and strategic mine planning uncertainty and risk management models*, Perth, WA, November 2004.

Jean-Paul Chilès and Pierre Delfiner. *Geostatistics: Modeling Spatial Uncertainty, 2nd Edition*. Wiley-Blackwell, 2012.

E.J. Cowan, R.K. Beatson, H.J. Ross, W.R. Fright, T.J. McLennan, T.R. Evans, J.C. Carr, R.G. Lane, D.V. Bright, A.J. Gillman, P.A. Oshust, and M. Titley. Practical implicit geological modelling. In *5th International Mining Geology Conference*, Bendigo, Victoria, November 2003. The Australian Institute of Mining and Metallurgy.

Miguel de la Varga and J. Florian Wellmann. Structural geologic modeling as an inference problem: A bayesian perspective. *Interpretation*, 4(3):1 – 16, 2016.

Charles R. Ehlschlaeger, Ashton M. Shortridge, and Michael F. Goodchild. Visualizing spatial data uncertainty using animation. *Computers & Geosciences*, 23:387 – 395, 1997.

Ayres C. Fan, John W. Fisher III, William M. Wells III, James J. Levitt, and Alan S. Willsky. Mcmc curve sampling for image segmentation. In *Medical Image Computing and Computer-Assisted Intervention – MICCAI 2007*, Brisbane, Australia, October 29 - November 2 2007. Springer.

Tobias Frank, Anne-Laure Tertois, and Jean-Laurent Mallet. 3d-reconstruction of complex geological interfaces from irregularly distributed and noisy point data. *Computers & Geosciences*, 33: 932 – 943, 2007.

Frederic Gibou, Ronald Fedkiw, and Stanley Osher. A review of level-set methods and some recent applications. *Journal of Computational Physics*, 353:82 – 109, 2018.

Ítalo Gomes Gonçalves, Sissa Kumaira, and Felipe Guadagnin. A machine learning approach to the potential-field method for implicit modeling of geological structures. *Computers & Geosciences*, 103:173 – 182, 2017.

Peter J. Green. Reversible jump markov chain monte carlo computation and bayesian model determination. *Biometrika*, 82:711 – 732, 1995.

L. Grose, G. Laurent, L. Aillères, R. Armit, M. Jessell, and T. Cousin-Dechenaud. Inversion of structural geology data for fold geometry. *Journal of Geophysical Research: Solid Earth*, 2018. doi: https://doi.org/10.1029/2017JB015177.

Thomas Mejer Hansen, Knud Skou Cordua, and Klaus Mosegaard. Inverse problems with non-trivial priors: efficient solution through sequential gibbs sampling. *Solid Earth*, 16:593 – 611, 2012.

Imen Hassen, Helen Gibson, Fadoua Hamzaoui-Azaza, François Negro, Khanfir Rachid, and Rachida Bouhlila. 3d geological modeling of the kasserine aquifer system, central tunisia: New insights into aquifer-geometry and interconnections for a better assessment of groundwater resources. *Journal of Hydrology*, 539:223 – 236, 2016.

Lars Holden, Petter Mostad Bjørn, Fredrik Nielsen, Jon Gjerde, Chris Townsend, and Signe Ottesen. Stochastic structural modeling. *Mathematical Geology*, 35:899 – 914, 2003.

Weisheng Hou, Liang Yang, Dongcheng Deng, Jing Ye, Keith Clarke, Zhijun Yang, Wenming Zhuang, Jianxiong Liu, and Jichun Huang. Assessing quality of urban underground spaces by

coupling 3d geological models: The case study of foshan city, south china. *Computers & Geosciences*, 89:1 – 11, 2016.

Lin Y. Hu. Gradual deformation and iterative calibration of gaussian-related stochastic models. *Mathematical Geology*, 32:87 – 108, 2000.

David A. B. Hyde, Tyler R. Hall, and Jef Caers. VRGE: An immersive visualization application for the geosciences (in press). In *2018 IEEE Scientific Visualization Conference (SciVis)*, Oct 2018.

Marco A. Iglesias, Yulong Lu, and Andrew M. Stuart. A bayesian level set method for geometric inverse problems. *Interfaces and Free Boundaries*, 18:181 – 217, 2016.

P. Jones, I. Douglas, and A. Jewbali. Modeling combined geological and grade uncertainty: Application of multiple-point simulation at the apensu gold deposit, ghana. *Mathematical geosciences*, 45:949 – 965, 2013.

Olivier Juan, Renaud Keriven, and Gheorghe Postelnicu. Stochastic motion and the level set method in computer vision: Stochastic active contours. *International Journal of Computer Vision*, 69:7 – 25, 2006.

Phaedon C. Kyriakidis and André G. Journel. Geostatistical space–time models: A review. *Mathematical geology*, 31:654 – 684, 1999.

Christian Lajaunie, Gabriel Courrioux, and Laurent Manuel. Foliation fields and 3d cartography in geology: Principles of a method based on potential interpolation. *Mathematical Geology*, 29: 571 – 584, 1997.

Magali Lecour, Richard Cognot, Isabelle Duvinage, Pierre Thore, and Jean-Claude Dulac. Modelling of stochastic faults and fault networks in a structural uncertainty study. *Petroleum Geoscience*, 7:31 – 42, 2001.

Mark D. Lindsay, Laurent Aillères, Mark W. Jessell, Eric A. de Kemp, and Peter G. Betts. Locating and quantifying geological uncertainty in three-dimensional models: Analysis of the gippsland basin, southeastern australia. *Tectonophysics*, 546-547:10 – 27, 2012.

M.D. Lindsay, M.W. Jessell, L. Ailleres, S. Perrouty, E.de Kemp, and P.G. Betts. Geodiversity: Exploration of 3d geological model space. *Tectonophysics*, 594:27 – 37, 2013.

Jean-Laurent Mallet. *Elements of Mathematical Sedimentary Geology: the GeoChron Model*. EAGE, 2014.

Gregoire Mariethoz and Jef Caers. *Multiple-point Geostatistics: Stochastic Modeling with Training Images*. Wiley-Blackwell, 2015.

Jyotiprasad Medhi. *Stochastic Processes*. New Age International, 1994.

David L. Moreno and Sigurd I. Aanonsen. Continuous facies updating using the ensemble kalman filter and the level set method. *Mathematical Geosciences*, 43:951 – 970, 2011.

Klaus Mosegaard and Malcolm Sambridge. Monte carlo analysis of inverse problems. *Inverse Problems*, 18, 2002.

Ken Museth, Ross Whitaker, and David Breen. Editing geometric models. In *Geometric Level Set Methods in Imaging, Vision, and Graphics*. Springer, New York, 2003.

Henning Omre. Bayesian kriging—merging observations and qualified guesses in kriging. *Mathematical geology*, 19:25 – 39, 1999.

Stanley Osher and Ronald Fedkiw. *Level set methods and dynamic implicit surfaces*, volume 153 of *Applied Mathematical Sciences*. Springer, 2002.

Stanley Osher and James A. Sethian. Fronts propagating with curvature-dependent speed: Algorithms based on hamilton-jacobi formulations. *Journal of Computational Physics*, 79(1):12 – 49, 1988.

Nicolas Remy, Alexandre Boucher, and Jianbing Wu. *Applied Geostatistics with SGeMS: A User's Guide*. Cambridge University Press, 2009.

Per Røe, Frode Georgsen, and Petter Abrahamsen. An uncertainty model for fault shape and location. *Mathematical Geosciences*, 46(8):957 – 969, 2014.

L. C. G. Rogers and David Williams. *Diffusions, Markov Processes, and Martingales: Volume 1, Foundations*. Cambridge University Press, 2nd edition, 2000.

Céline Scheidt, Lewis Li, and Jef Caers. *Quantifying uncertainty in subsurface systems*. American Geophysical Union, Wiley, 2018.

C.E. Shannon. A mathematical theory of communication. *Bell System Technical Journal*, 27:379 – 423, 1948.

L. Tacher, I.Pomian-Srzednicki, and A.Parriaux. Geological uncertainties associated with 3-d subsurface models. *Computers & Geosciences*, 32:212 – 221, 2006.

Pierre Thore, Arben Shtuka, Magali Lecour, Taoufik Ait-Ettajer, and Richard Cognot. Structural uncertainties: Determination, management, and applications. *GEOPHYSICS*, 67(3):840 – 852, 2002.

Stefan A. Vollgger, Alexander R. Cruden, Laurent Ailleres, and E. Jun Cowan. Regional dome evolution and its control on ore-grade distribution: Insights from 3d implicit modelling of the navachab gold deposit, namibia. *Ore Geology Reviews*, 69:268 – 284, 2015.

J. Florian Wellmann and Klaus Regenauer-Lieb. Uncertainties have a meaning: Information entropy as a quality measure for 3-d geological models. *Tectonophysics*, 526-529:207 – 216, 2012.

J. Florian Wellmann, Franklin G. Horowitz, Eva Schill, and Klaus Regenauer-Lieb. Towards incorporating uncertainty of structural data in 3d geological inversion. *Tectonophysics*, 490:141 – 151, 2010.

J. Florian Wellmann, Miguel de la Varga, Ruth E. Murdie, Klaus Gessner, and Mark Jessell. Uncertainty estimation for a geological model of the sandstone greenstone belt, western australia – insights from integrated geological and geophysical inversion in a bayesian inference framework. In *Special Publications*, London, October 2017. Geological Society.

Jiang Xie, Yalchin Efendiev, and Akhil Datta-Gupta. Uncertainty quantification in history matching of channelized reservoirs using markov chain level set approaches. In *SPE Reservoir Simulation Symposium*, Woodlands, Texas, USA, February 2011. Society of Petroleum Engineers.

Hong-Kai Zhao, Stanley Osher, and Ronald Fedkiw. Fast surface reconstruction using the level set method. In *IEEE Workshop on Variational and Level Set Methods in Computer Vision*, pages 194–201. IEEE, 2001.